Atomic layer deposition of InN using trimethylindium and ammonia plasma

Petro Deminskyi[a)], Polla Rouf, Ivan G. Ivanov, Henrik Pedersen

Department of Physics, Chemistry and Biology, Linköping University, SE-58183 Linköping, Sweden

[a)] Electronic mail: petro.deminskyi@liu.se

InN is a low band gap, high electron mobility semiconductor material of interest to optoelectronics and telecommunication. Such applications require the deposition of uniform crystalline InN thin films on large area substrates, with deposition temperatures compatible with this temperature-sensitive material. As conventional chemical vapor deposition (CVD) struggles with the low temperature tolerated by the InN crystal, we hypothesize that a time-resolved, surface-controlled CVD route could offer a way forward for InN thin film deposition. In this work, we report atomic layer deposition of crystalline, wurtzite InN thin films using trimethylindium and ammonia plasma on Si(100). We found a narrow ALD window of 240–260 °C with a deposition rate of 0.36 Å/cycle and that the flow of ammonia into the plasma is an important parameter for the crystalline quality of the film. X-ray diffraction measurements further confirmed the polycrystalline nature of InN thin films. X-ray photoelectron spectroscopy measurements show nearly stoichiometric InN with low carbon level (< 1 atomic %) and oxygen level (< 5 atomic %) in the film bulk. The low carbon level is attributed to a favorable surface chemistry enabled by the NH_3 plasma. The film bulk oxygen content is attributed to oxidation upon exposure to air via grain boundary diffusion and possibly by formation of oxygen containing species in the plasma discharge.

I. INTRODUCTION

Indium nitride (InN) has interesting optical and electronic properties such as low energy band-gap (0.7 eV), very high electron mobility (theoretical maximum

~4400 $cm^2/V\times s$) and high electron saturation velocity (4.2×10^7 cm/s) making it an attractive material for e.g. high frequency electronics and lasers.[1,2] Chemical vapor deposition (CVD) of InN using trimethylindium, ($In(CH_3)_3$, TMI) and ammonia (NH_3), as precursors is limited by the thermal stability of the InN crystal above 500 ºC, as it decomposes to In metal and N_2 gas at those temperatures.[3] This combined with the TMI decomposition (that occurs homogeneously in the temperature range 120−535 ºC),[4] and low reactivity of NH_3 at temperatures below 500 ºC,[5] force the use of N/In ratios as high as 10^5 in CVD of InN.[6] We hypothesize that a better route would be a surface-controlled CVD process where the role of the gas phase chemistry is strongly reduced or even eliminated. A time-resolved CVD route, where the In and N precursors are separated in time to promote a kinetically-controlled pulsed process, could be such a route. Therefore, a time-resolved CVD process in the form of atomic layer deposition (ALD) for InN was explored. Given the low reactivity of ammonia at low temperatures, a nitrogen containing plasma has been used in previous studies for ALD of both polycrystalline and epitaxial InN on different planar and 3D substrate topographies.[7-11] The literature on InN ALD uses mainly TMI as In precursor, with InCp as a notable exception.[12] It has been shown that Ar-N_2 plasma and TMI, results in a poorly functioning surface chemistry for removal of methyl groups from the surface, and requires very long plasma exposures, up to 120 s.[9,11] *Nepal et al.* reported a correlation between changes in the gas-phase chemistry of the plasma source and InN film; higher nitrogen atom concentration within the plasma source is correlated with smoother InN films. Furthermore, low N_2 flow appears to aid reduction of the carbon content.[10] The use of ammonia plasma as an alternative nitrogen source for InN ALD has not been fully investigated, although briefly mentioned by *Ozgit-Akgun et al*.[12] The approach to InN ALD employing $In(CH_3)_3$ is interesting since the NH_x species present in the plasma are believed to remove hydrocarbons from the surface.[13] In this work, we report on the self-limiting growth of crystalline InN thin films by ALD using TMI and ammonia plasma. Additionally, the impact of ammonia plasma power and ammonia flow on film quality has been investigated, analyzed and described in detail.

II. EXPERIMENTAL

A. Film deposition

Depositions were carried out in a Picosun R-200 atomic layer deposition tool without load lock chamber with a total pressure of 6 hPa. The ICP plasma is generated within a quartz tube surrounded by a cylindrical RF coil. The substrate holder stage is located downstream (~70 cm) from the plasma source. ALD of InN were conducted within the temperature range of 200–360 ºC on 2×2 cm Si(100) using NH_3 plasma, and $In(CH_3)_3$, kept in a stainless-steel bubbler mounted in a Peltier element with the temperature set at 23 ºC. N_2 (99.999 %) was used as the carrier gas for trimethylindium precursor delivery to the reaction chamber. The plasma was ignited using a co-flow of 100 sccm Ar (99.9997 %) together with the NH_3 (99.999990 %) flow. N_2, Ar, and NH_3 gases were further purified by getter filters. The gas mixture was fed into the system downstream from the ICP source. Unless stated otherwise, the NH_3 flow rate was 50 sccm and the plasma power in the range from 2400 W to 2800 W with 10 s plasma pulses. An AB-type ALD process was used with TMI and NH_3 plasma. The TMI vapor pressure is given by Eqn. (1)[14]:

$$log\ P\ (Torr) = 10.98 - \frac{3204}{T\ (K)}, \quad (1)$$

which gives the vapor pressure of TMI to 1.46 hPa at 23 ºC, which is lower than the total pressure in the deposition chamber. We therefore used a bubbler "fill-empty" approach for the TMI exposure: During the first pulse, the fill-pulse, the ALD valve is opened and a high flow of 300 sccm nitrogen carrier gas is passing through the bubbler. The high flow increases the total pressure in the bubbler. The partial pressure of the TMI in the bubbler is not expected to be affected by this. Then in the second pulse, the empty-pulse, the ALD valve is opened to the bubbler and a low flow of 100 sccm nitrogen carrier gas is flown through the bubbler. The high pressure in the bubbler, created by the high nitrogen flow in the fill-pulse, serves to empty the bubbler into the reaction chamber. This can be noted by carefully monitoring the pressure in the growth chamber; a short increase in pressure can be noted during the empty-pulse. The two pulses are separated by 10 s to allow gas mixing in the bubbler. The pulse times used in the fill-empty of the process was 4 s for the fill sub-pulse and a variable time for the empty sub-pulse. A 10 s

purge was used after the TMI fill-empty pulse sequence followed by 10 s NH_3 plasma exposure, unless otherwise noted, and 6 s purge to complete the ALD cycle.

Prior to deposition, the Si(100) substrate was cleaned in acetone, 2-propanol and deionized (DI) water with further sample drying under N_2 flow. Silicon substrates were transferred into the ALD chamber which was held at the set deposition temperature. An in-situ surface pretreatment with 2800 W N_2 plasma for 2 min was conducted to make the substrate surface somewhat more nitrogen-rich before InN growth. Post-deposition annealing of some InN films was done in the reactor prior to unloading the sample by increasing the temperature to 500 ºC for 2 hours at 10 sccm N_2 flow.

B. Film characterization

X-ray diffraction (XRD) analysis was performed by using Empyrean PanAnalytical X'Pert system with a Philips Bragg–Brentano diffractometer that was equipped with a parallel beam detector. The Cu Kα radiation source (λ=0.154[06] nm) was operated at 40 kV and 40 mA. The grazing incidence X-ray diffraction (GIXRD) mode was used to minimize the intensity from the substrate peaks since the films were limited in thickness. The incoming beam angle, ω, was 0.5º. Data were obtained within the 2θ range of 20–90º, which were performed using 0.02º step size and 1 s step time. Interplanar spacing (d_{hkl}) values were calculated from peaks position using Bragg's law for hexagonal lattice. Lattice parameters *a* and *c* were calculated by substituting d_{hkl} values using Eqn. (2).

$$\frac{1}{d^2} = \frac{4}{3}\left(\frac{h^2+hk+k^2}{a^2}\right) + \frac{l^2}{c^2}. \qquad (2)$$

Thickness and film density of the deposited films where measured by a PanAnalytical X'Pert Pro in the X-ray reflectometry (XRR) mode. Growth rates were calculated by dividing film thicknesses by the number of ALD cycles. Surface morphologies of InN thin films were studied using a high-resolution LEO 1550 Gemini field emission SEM. Chemical composition and bonding states of the films were determined by an Axis Ultra DLD instrument from Kratos Analytical X-ray photoelectron spectroscopy (XPS) with a base pressure of 1.1×10^{-9} Torr (1.5×10^{-7} Pa) and monochromatic Al K_a source (h_υ=1486.6 eV). Depth profiling was carried out using an Ar ion sputter beam with an acceleration voltage, spot size, and a sputtering time

duration of 0.5 kV, 300×700 μm, and 400 s respectively. Spectra deconvolution and quantification were performed using Casa XPS software.

The Raman spectra are measured in a micro-Raman setup in the wavelength range 72–1624 cm^{-1} using excitation of 532 nm. The laser (with power of 1 mW to avoid thermal damage to the sample) is focused on the sample to a spot of diameter ~0.85 μm using a microscope objective with magnification 100X and numerical aperture 0.95. The detection of the spectra is done with a single monochromator (Jobin-Yvon, Model HR460) equipped with a 1200 grooves/mm grating and a CCD camera. The resulting resolution of the system is ~2.5 cm^{-1}. Owing to the small thickness of the InN layers, the spectrum is strongly dominated by the Raman scattering from the Si-substrate. Nevertheless, it is possible to distinguish clearly the contribution from the InN layer, as will be discussed later.

Ellipsometric spectra of the films were recorded in the wavelength range of 200–1500 nm at three angles of incidence (65º, 70º, and 75º) by using a variable angle spectroscopic ellipsometer (J.A. Woollam). Optical constants of the InN thin films were modeled by the Tauc-Lorentz function as an oscillator. The absorption coefficient,

$$\alpha(\lambda) = \frac{4\pi k(\lambda)}{\lambda} \quad (3)$$

was calculated from the values of the extinction coefficient $k(\lambda)$ determined from the measured ellipsometry data. Optical band gap (E_g) is expressed by the following equation for direct band gap materials and was analytically extracted via extrapolation of the linear part of the absorption spectrum to $(\alpha E)^2 = 0$, where E denotes the photon energy.

$$\alpha E = A(E - E_g)^{1/2}. \quad (4)$$

C. Plasma characterization

Optical emission spectroscopy (OES) was performed using the Mechelle 900 Spectrometer with cooled digital 12-bit CCD camera system with a wavelength range of UV–NIR (200–1100 nm), mounted perpendicularly to the plasma source. Light emitted from the NH_3 plasma was collected and directed to a monochromator with an optical fiber cable. The optical emission from the plasma was measured just after the ICP source in the gas flow direction, before the plasma reached the substrate. Data was analyzed with consideration for spectrometer spectral resolution of 900 (meaning that two wavelengths separated by 1/900 of

the wavelength can be resolved). The measure of resolution is a constant of the instrument, which implies that the fractional wavelength resolution does not vary with the wavelength. The plasma diagnostics were focused on the formation of NH, N_2, N_2^+, and H, at different plasma power, NH_3 flow rate, and their influence on InN properties.

III. RESULTS AND DISCUSSION

The InN deposition process was studied by varying the second sub-pulse, i.e. the empty sub-pulse of the TMI fill-empty pulse between 0 and 6 s, while keeping the fill sub-pulse at 4 s and the NH_3 pulse at 10 s, or by keeping the fill sub-pulse at 4 s, the empty sub-pulse at 3.5 s and varying the NH_3 plasma pulse between 0 and 20 s. For all experiments, the purge times (6 s), deposition temperature (300 ºC) and plasma power (2400 W) were kept constant. The conventional ALD cycles with a single step TMI pulse, i.e. only a 4 s fill sub-pulse, did not afford uniform InN growth on Si(100) substrates. We ascribe this to insufficient TMI vapor delivery. Figure 1a shows the effect of the time for both the TMI pulse and the NH_3 plasma pulse on the growth rate of InN. A second set of experiments (Fig. 1b) studied the effect of the deposition temperature on the InN growth. Here the TMI empty pulse was 3 s and the NH_3 plasma pulse 10 s while varying the temperature from 200 ºC to 360 ºC.

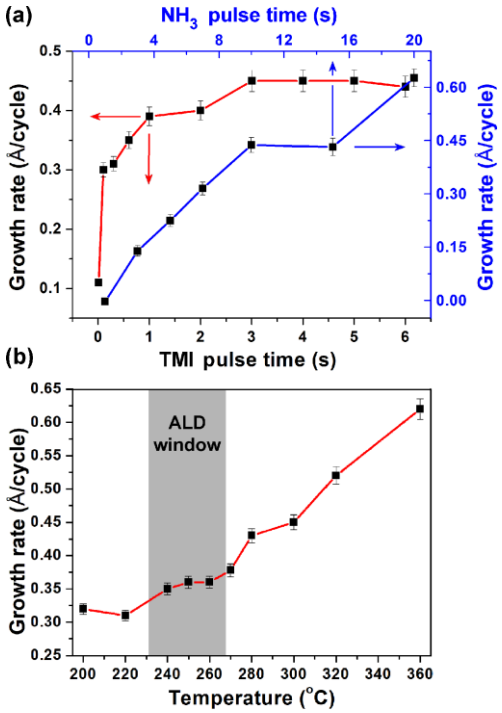

FIG. 1. (a) Effect of TMI and NH_3 precursors dose time on InN growth rate with 2400 W plasma power at 300 ºC with 10 s NH_3 pulse (red line), and 2800 W plasma power at 320 ºC with 3.5 s TMI empty sub-pulse (blue line). (b) Effect of temperature on growth rate, for 3 s TMI empty sub-pulse and 10 s NH_3 pulse. The TMI fill sub-pulse was 4 s for all experiments.

The results on InN growth rate as a function of a growth temperature (within 200–360 °C) show that InN is deposited at 200 °C with 0.32 Å/cycle. The growth rate increases with temperature and shows a narrow plateau of 0.36 Å/cycle at 240–260 ºC which could be regarded as a narrow ALD temperature window. It should, however, be noted that the saturation curves are done at higher temperatures, 300 ºC and 320 ºC, demonstrating that the deposition chemistry is self-limiting also at these higher temperatures. The growth rate then further increases to reach 0.62 Å/cycle at 360 ºC (Fig. 1b). This indicates saturation in growth rate both as a function of the precursor pulse time and of the temperature. The ALD-cycle for further experiments were set to: TMI 4 s fill sub-pulse and 3.5 s empty sub-pulse, 10 s purge, 10 s NH_3 plasma and 6 s purge.

Figure 3 displays the SEM images of InN morphology for films deposited at 300 °C with various durations of the TMI empty sub-pulses. Without the use of fill-empty for the

TMI pulse, the deposition process leads to growth of isolated islands (Fig. 2a). By only adding a 0.1 s empty sub-pulse, the islands coalesce (Fig. 2b). Longer empty sub-pulses lead to growth of continuous films consisting of smaller and smaller grains with longer time for the empty sub-pulse. We interpret this as insufficient TMI delivery without the empty sub-pulse.

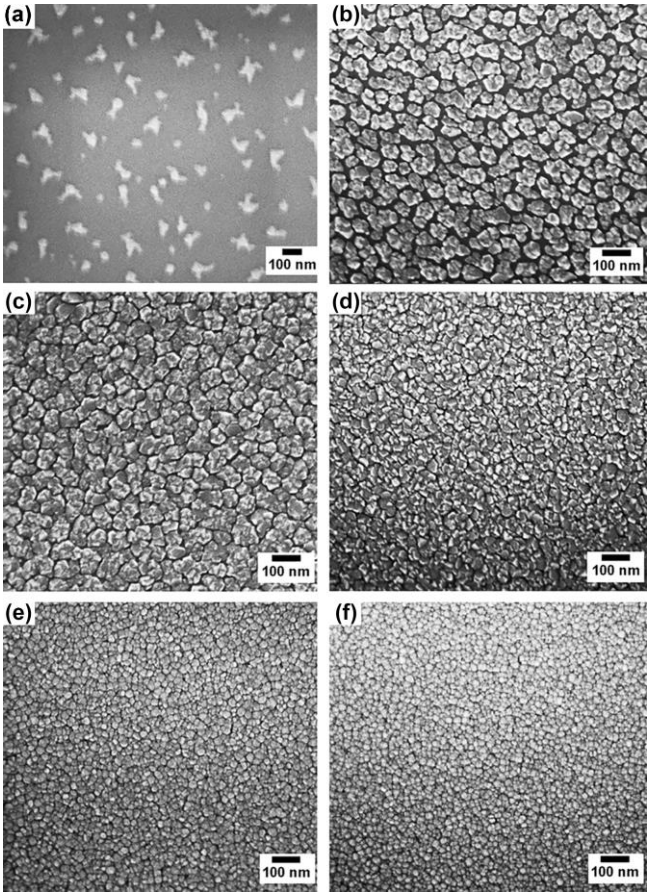

FIG. 2. Top view SEM images of InN film deposited at 300 ºC for various times of the TMI empty sub-pulse: 0 s (a), 0.1 s (b), 0.3 s (c), 0.6 s (d), 1 s (e), and 6 s (f).

Figure 3 displays the SEM images of crystalline grain structures of InN films deposited at 200 ºC, 260 ºC, 300 ºC, and 360 ºC with 2400 W plasma power. Changing the temperature leads to the formation of larger grains and their coalescence into larger clusters and a surface morphology characterized by voids between them especially large voids pronounced at 360 ºC. It should be noted here that the aim of this study has been to investigate how to deposit the best possible InN material, suitable for use in electronic devices. For such applications, the crystalline quality and the amount of impurities must

be reduced. We have therefore focused most of our efforts to a deposition temperature of 320 °C. Figure 4 displays the SEM images of crystalline grain structures of InN films deposited with 2400 W, 2500 W, 2700 W, and 2800 W plasma power at 320 °C. Changing the plasma power does not have a clear impact on the film morphology, while the GIXRD shows a change in crystalline quality (Fig. 6b). The growth rate changes somewhat with the plasma power from 0.51±0.03 Å/cycle at 2400 W to 0.47±0.03 Å/cycle at 2800 W. Figure 5 shows SEM images of InN films deposited with 50 sccm, 75 sccm, 100 sccm ammonia flow under 2800 W plasma power at 320 °C. Changing ammonia flow has slight impact on the film morphology in terms of grains crystallization. The GIXRD results and variations of the *a*- and *c*-axis lattice constants show a change in crystalline quality of InN (Fig. 6b). The growth rate changes somewhat with the ammonia flow from 0.44 Å/cycle at 50 sccm to 0.33 Å/cycle at 100 sccm. This could be explained by an increased density of hydrogen radicals in ammonia plasma with higher ammonia flow rate as hydrogen radicals has been shown to reduce the growth rate of InN films.[15]

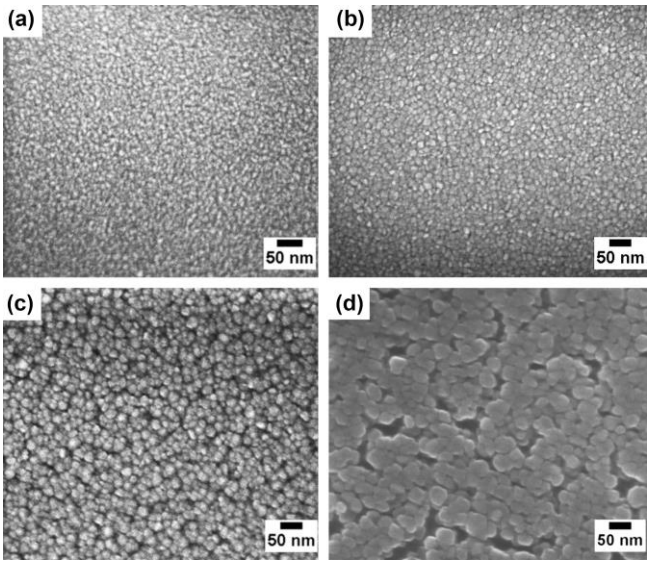

FIG. 3. Top view SEM images of InN films deposited at 200 ºC (a), 260 ºC (b), 300 ºC (c), and 360 ºC (d) with 2400 W plasma power.

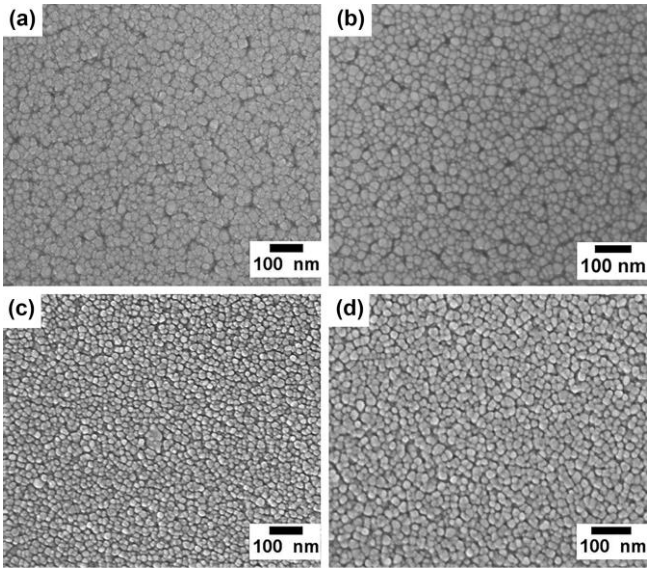

FIG. 4. Top view SEM images of InN films deposited at 2400 W (a), 2500 W (b), 2700 W (c), and 2800 W (d) plasma power at 320 °C.

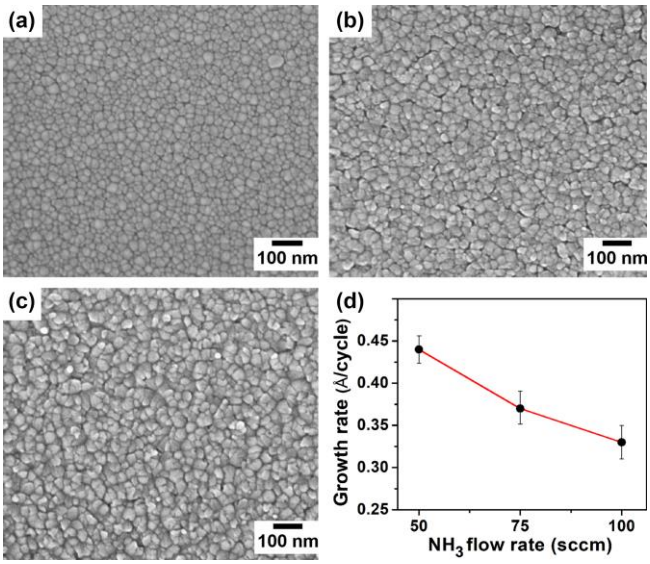

FIG. 5. Top view SEM images of InN films for 50 sccm (a), 75 sccm (b) and 100 sccm (c) of NH_3 flow. (d) Effect of NH_3 flow on InN growth rate with 2800 W plasma power at 320 ºC.

The crystallinity of the InN films studied by GIXRD is shown in Figure 6a for 18 nm, 26 nm and 31 nm thick films deposited with 2400 W plasma power at 240 ºC, 320 ºC, and 360 ºC, respectively. Figure 6b shows the GIXRD measurements of 26 nm, 25 nm and 23 nm thick InN films deposited at 320 ºC with 2400 W, 2500 W, and 2800 W

plasma power, respectively. The (100), (002), (011), (012), (110), (013), (020), (004) and (023) reflections[16,17] of the hexagonal wurtzite phase of InN were observed. We note that changes in deposition temperature and plasma power do not alter the peak positions, while the intensity of the peaks increases with increasing deposition temperature. The lattice parameters *a* and *c* were calculated using Eqn. (2) and the 2θ positions of the (002) and (011) reflections (Fig. 7a,b and Fig. 8b). Interplanar spacing (d_{hkl}) values of (002) and (011) planes were calculated from Bragg's law. The relation between the strain in the *c*-axis direction $\varepsilon_c = |(c-c_0)/c_0|$ and that in the direction of the a-axis $\varepsilon_a = |(a-a_0)/a_0|$, (where c_0=5.7033 Å and a_0=3.5378 Å correspond to epitaxial InN) gives values ~0.004 for ε_c and 0.002 for ε_a indicating almost fully relaxed and strain free InN films (Fig. 7a,b and Fig. 8b).[18,19] It should be noted that the strain in the c-axis and a-axis being calculated in all cases is for the individual grains of the polycrystalline material.

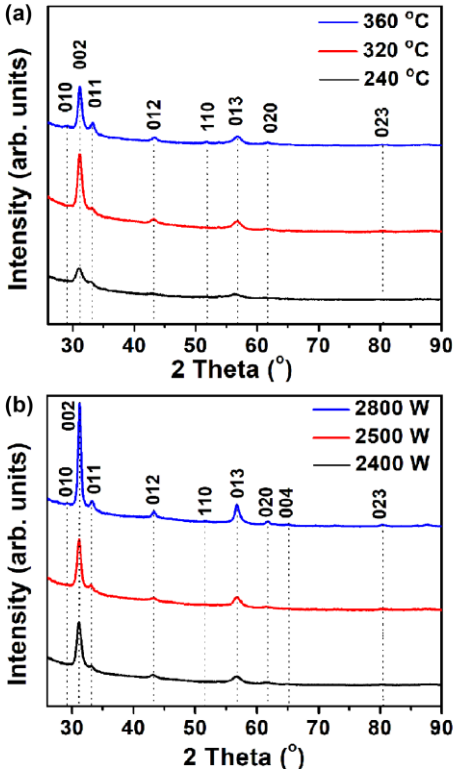

FIG. 6. GIXRD pattern of InN film deposited on Si(100) substrate (a) under 240 ºC, 320 ºC, 360 ºC deposition temperatures and 2400 W plasma power; (b) under 2400 W, 2500 W, 2800 W plasma power and 320 ºC deposition temperature.

GIXRD of InN thin films grown with 2400 W NH_3 plasma power at 240 ºC, 320 ºC, and 360 ºC indicated that with higher temperature, the *c*-axis and *a*-axis lattice parameters are shifting towards the values that corresponding to the fully relaxed and strain free InN films (Fig. 7a). Furthermore, the investigation of crystalline quality of InN films grown under 2400 W, 2500 W, 2800 W plasma power and 320 ºC deposition temperature indicate that *c*-axis and *a*-axis lattice parameters keep shifting towards *c*-axis and *a*-axis lattice parameters that corresponding to the single crystal InN film (Fig. 7b). GIXRD of ~40 nm and ~49 nm InN thin films grown with 2800 W NH_3 plasma power at 320 ºC, and 360 ºC with an added annealing at 500 ºC for 2 h indicated that the annealing affected the relative intensities of the peaks. For the InN films grown at 320 ºC (~40 nm), and 360 ºC (~49 nm), the *c*-axis lattice parameter was 5.7140 Å and 5.7058 Å while the *a*-axis lattice parameter was 3.5198 Å and 3.5254 Å, showing that the annealing further reduces the stress in the material. GIXRD measurements of InN films grown with different ammonia flows (Fig. 8a, Fig. S1) show that the diffraction peaks intensities increase with higher ammonia flow, and that the *a*- and *c*-axis lattice have values of 3.5427 Å and 5.6998 Å at the optimal ammonia flow. This indicate slight switch from tensile to compressive strain in the *c*-axis direction for the individual grains of the InN films grown at 75 sccm and 100 sccm NH_3 flow, respectively, and an increased crystalline quality of InN with higher ammonia flow in the plasma. All values of *a*- and *c*-axis lattice parameters are summarized in the Table S1. XRR for ~35 nm-thick InN film deposited with 100 sccm NH_3 flow under 2800 W plasma power at 320 ºC reveals film density of 6.47 g/cm^3 which is in agreement with previously reported values.[9,20]

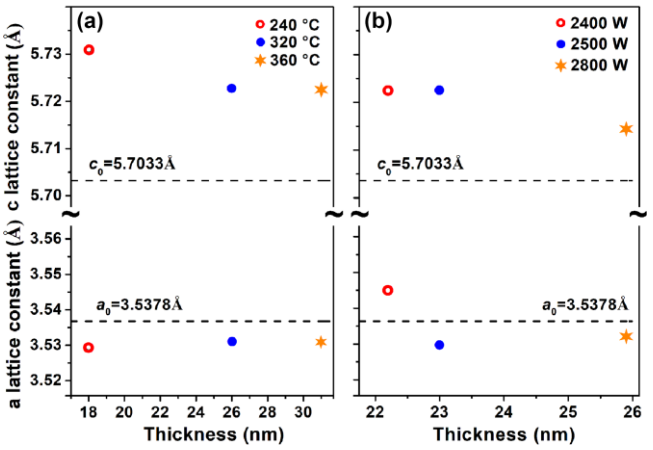

FIG. 7. Variations of the *a*- and *c*-axis lattice constants of In- and N-growth face InN films with the film thickness at (a) different temperatures at 2400 W NH_3 plasma, and (b) different plasma power at 320 ºC. Dashed lines show strain-free lattice constant of the *a*- and *c*-axis.[18]

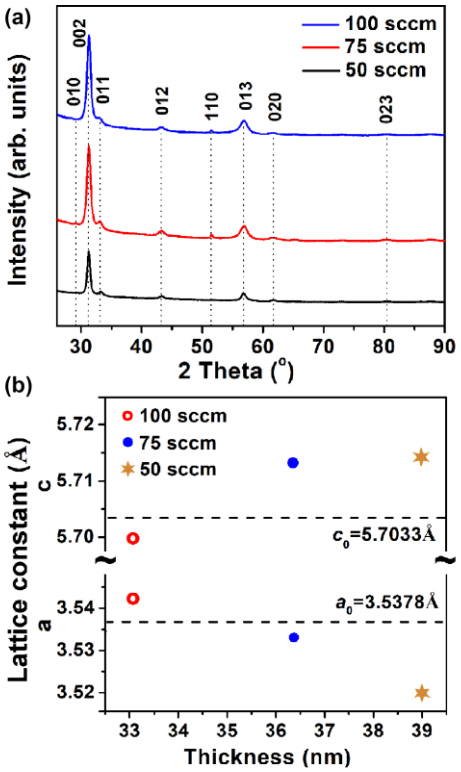

FIG. 8. GIXRD pattern (a) and variations of the *a*- and *c*-axis lattice constants (b) of InN film deposited on Si(100) substrate at 50 sccm, 75 sccm and 100 sccm of NH_3 flow with 2800 W plasma power at 320 ºC. (More detailed information on peak intensities of GIXRD pattern is summarized in Fig. 1S).

XPS measurements were conducted on InN thin films grown at 320 ºC with and without a subsequent annealing at 500 ºC. Figure 9 shows the narrow scan XPS of In 3d and N 1s spectra for different growth and post-treatment temperatures which refer to the bulk film (t_{etch} = 400 s), and which is in agreement with previously reported values.[9,21] The surface of the InN film is oxidized and carbonized (~30% oxygen and ~25% carbon) is likely to originate from post-deposition exposure to atmosphere. For compositional depth profile measurements, InN thin films were etched by Ar^+ ions in steps of 400 s to obtain elemental composition from the bulk of the films. While carbon is detected on the films surface, the carbon signal is below the XPS detection limit in the bulk of the InN films. This is indicative of a well-functioning surface chemistry with the ammonia plasma, aiding in the removal of the methyl groups on the surface.[22] Significant amounts of oxygen (O) were detected in the bulk of the film, (Table I). This could be caused by oxygen containing species formed in the quartz tube of the inductively coupled plasma source.[10] The polycrystalline nature of the films could also lead to oxidation of the film bulk via oxygen diffusion in grain boundaries. Figure 3a-d and Figure 6a show larger grain size and higher crystalline quality with higher deposition temperature, indicating that the lower oxygen content could be caused by less oxygen diffusion into the film with the larger crystallites. The In/N ratio was computed from the composition of InN thin films (Table I) indicating nitrogen deficient films.

TABLE I. Elemental compositions (at.%) and In/N ratios obtained from XPS survey spectra. The films are deposited with 2400 W plasma power and 50 sccm NH_3 flow.

Deposition temperature	**Surface**					**Bulk**				
	In	N	O	C	In/N Ratio	In	N	O	C	In/N Ratio
320 ºC	29.3	18.7	27.1	24.8	1.57	47.5	28.9	23.6	–	1.64
320 ºC annealed at 500 ºC	28.6	15.1	30.9	25.4	1.9	45.9	28.6	25.4	–	1.59

The In 3d XPS spectrum (Fig. 9) show two spin-orbit doublets; $In3d_{5/2}$ and $In\ 3d_{3/2}$ (with intensity ratio 3:2) for InN thin films grown at 320 ºC with and without a subsequent annealing at 500 ºC. The sub-peaks of the $In\ 3d_{5/2}$ and $In\ 3d_{3/2}$ correspond to In-N bonds and In-O bonds (Table II). The N 1s XPS spectrum reveal a dominant sub-

peak corresponding to N-In bonds which is more intense than the sub-peak corresponding to N-O bonds. A slight shift from higher to lower binding energies for N 1s peaks was observed when the deposition temperature was increased. This was correlated to the lower stress (higher crystallinity of InN) and lower oxygen content in the InN film (Fig. 8a,b) and stoichiometries closer to 1:1 (In:N) ratio that were obtained at higher deposition temperatures.

TABLE II. Binding energies obtained from XPS survey spectra of InN in the bulk.[9,21]

Deposition temperature	**Binding energy, eV**					
	In-N		In-O		N-In	N-O
	In $3d_{5/2}$	In $3d_{3/2}$	In $3d_{5/2}$	In $3d_{5/2}$	N 1s	
320 ºC	443.6	451.1	444.3	451.6	396.4	396.8
320 ºC annealed at 500 ºC	443.7	451.3	444.4	451.6	396.6	397.1

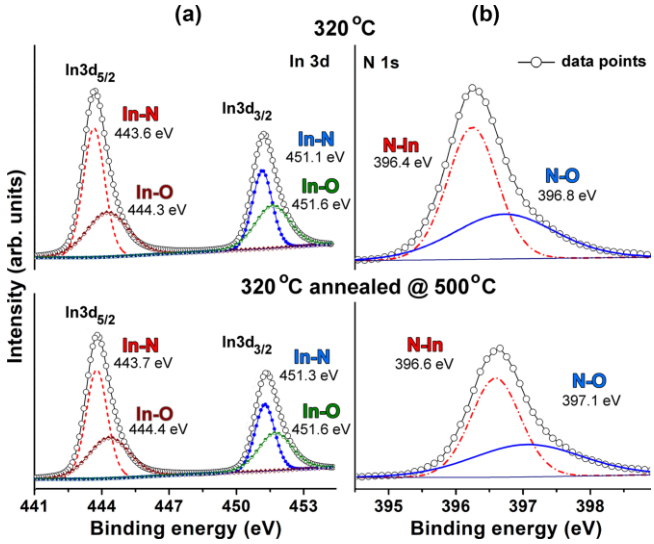

FIG. 9. High-resolution XPS spectra of (a) In 3d, (b) N 1s peaks of InN films deposited at temperatures. The spectra are taken after sputtering to represent the bulk of the films.

XPS measurements on InN films grown under 2800 W plasma power at 320 ºC show that a change in ammonia flow rate from 50 sccm to 75 sccm and further to 100 sccm, led to a significant reduction in oxygen content from ~24 at.% to ~5 at.% while the N content increased from ~29 at.% to ~44 at.%. The In/N ratio (Table III) indicating the shift from

highly nitrogen deficient films with In/N ratio of 1.64 (for 50 sccm ammonia flow) to a stoichiometry closer to 1 with In/N ratio of ~1.1 (for 75 sccm and 100 sccm). The lower oxygen content in the film bulk could be caused by the slightly larger crystalline grains formed with higher ammonia flow (Fig. 5a-c), which would lead to less grain boundary diffusion of oxygen. (Fig. 8). Another plausible reason for the lower oxygen content in the film bulk could be that the higher ammonia flow would reduce the impact of any oxygen containing species in the plasma discharge since a higher ammonia flow would render a lower partial pressure of the oxygen containing species. *Haider, et al.* for the ALD process with N_2 plasma after XPS analysis of InN films in the bulk have shown elemental composition of In (~65.0 at. %), N (~29.8 at. %), O (~2.1 at. %), C (~3 at. %) and In/N ration 2.17.[9] *Nepal et al.*, for the ALD process with N_2 plasma have shown that the In/N ratio is 1.46 at 260 °C.[11] The In/N ratio of 2.8 ± 0.7 has been reported on MBE grown InN.[23] Thus, the InN film grown in our study using NH_3 plasma has much better stoichiometry compared to MBE grown InN, better stoichiometry compared to N_2 plasma-assisted ALD processes reported by *Haider et. al.* and *Nepal et al.* at higher temperatures, and comparable stoichiometry compared to the values reported by *Nepal et al.* for InN grown at 190 ºC.

Table III. Elemental compositions (at.%) and In/N ratios obtained from XPS survey spectra. The films are deposited with 2800 W plasma power.

Deposition temperature	**Surface**					**Bulk**				
	In	N	O	C	In/N Ratio	In	N	O	C	In/N Ratio
50 sccm	29.3	18.7	27.1	24.8	1.57	47.5	28.9	23.5	–	1.64
75 sccm	22.9	21.7	25.8	29.4	1.05	46.2	41.2	11.5	1.0	1.12
100 sccm	23.9	22.5	25.3	28.2	1.06	50.8	43.8	4.8	0.53	1.15

In 3d XPS spectrum (Fig. 10) again show two spin-orbit doublets; In $3d_{5/2}$ and In $3d_{3/2}$ for InN thin films grown at 50 sccm, 75 sccm, 100 sccm of ammonia flow. The sub-peaks of the In $3d_{5/2}$ and In $3d_{3/2}$ correspond to In-N and In-O bonds (Table IV). The N 1s XPS spectrum reveal a dominant sub-peak corresponding to N-In bonds which is more intense than the sub-peak corresponding to N-O bonds. The binding energies as a function of different ammonia flow show slight shift to lower energies for peaks corresponding to In-N bonds. This is correlated to the lower oxygen content in the InN film for higher ammonia flow.

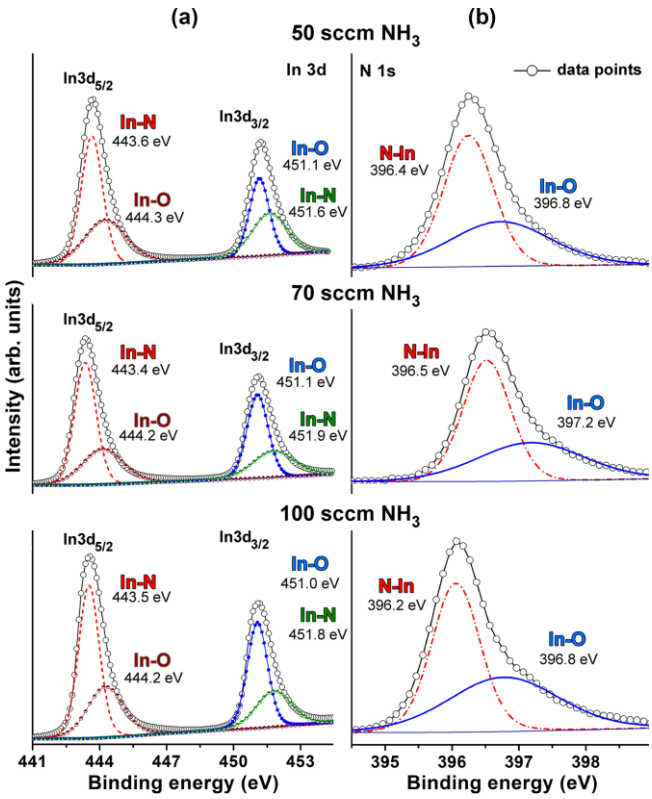

FIG. 10. High-resolution XPS spectra of (a) In 3d, (b) N 1s peaks of InN films deposited with 50 sccm, 75 sccm, 100 sccm of ammonia flow at 320 ºC and 2800 W of plasma power. The spectra are taken after sputtering to represent the analysis of InN in the bulk.

Table IV. Binding energies obtained from XPS survey spectra of InN in the bulk.[9,21]

NH_3 flow rate	**Binding energy, eV**					
	In-N		In-O		N-In	N-O
	In $3d_{5/2}$		In $3d_{3/2}$		In $3d_{5/2}$	In $3d_{5/2}$
50 sccm	443.6	451.1	444.3	451.6	396.4	396.8
75 sccm	443.4	451.1	444.2	451.9	396.5	397.2
100 sccm	443.5	451.0	444.2	451.8	396.2	396.8

To further understand the deposition process, we collected OES spectra during InN deposition at 320 ºC with plasma powers of 2400 W and 2800 W and with NH_3 flow rates of 50 sccm, 75 sccm and 100 sccm. A carrier flow of 100 sccm Ar was used for all experiments (see Fig. 11 and Table V). The emission spectra for the 2400 W and 2800 W of NH_3 plasmas were found to be very similar with the same peaks positions and almost the same peaks intensities. The prominent lines were observed as a line related to NH at

336.1 nm, a line related to N_2 at 357.1 nm, a shoulder related to CN at 388.5 nm, and a line related to N_2^+ at 391.4 nm. The NH, N_2, and N_2^+ species were not observed to increase with increased plasma power but with increased NH_3 flow rate (Fig. 11a, and Fig. 11b). The emission peaks at ~336 nm and 337 nm for different plasma power and NH_3/Ar flow rate, indicate the presence of the excited NH, N_2 radicals that corresponds to $A^3\Pi \rightarrow X^3\Sigma$ and $C^3\Pi_u \rightarrow B^3\,\Pi_g$ transitions, corroborating the presence of NH_x (x<3) and N_2 species.[24,25] In addition to NH, N_2, N_2^+, and CN detected in NH_3/Ar plasma, the H_γ, H_β, and H_α lines were detected at 434.0 nm, 486.1 nm, and ~656.3 nm (Table V). The presence of N_2, N_2^+ and H radicals can be attributed to the collisions of NH radicals: $NH+NH \rightarrow N_2+2H$ ($k = 1.2\times10^{-15} m^3s^{-1}$).[26] CN species are attributed to the plasma−surface interactions; species created at the surface in reactions with the ammonia plasma and surface bound methyl groups, which are then further decomposed in the plasma making them visible as CN in OES measurement, and then removed from the chamber during the purge step.[27] The OES measurements could not find any optically active oxygen containing species and can thus not confirm any formation of oxygen containing species in the plasma discharge in the quartz tube. It is important to note that the OES measurements only detect optically active species and possible oxygen containing species might not be optically active. The OES measurements are thus not suggesting that oxygen containing species are not formed in the plasma discharge.

Table V. Spectral characteristics of species detected in the NH_3/Ar plasma.

Species	λ, nm			Transition	Reference
NH	336.1			$A^3\Pi \rightarrow X^3\Sigma^-$(3360 Å system)	24
N_2	337.1,	357.7		$C^3\Pi_u \rightarrow B^3\,\Pi_g$ Second positive	24, 28, 29
N_2^+	391.4,	427.6		$B^2\Sigma_u^+ \rightarrow X^2\Sigma_g^+$	24, 28
CN	388.88			$B^2\Sigma_u^+ \rightarrow X^2\Sigma_g^+$	28, 30
H_γ, H_β, H_α	434.0,	486.1,	656.29	n(>2) → n = 2 (Balmer line)	29
	695.6,	750.3,	911.1	$4p^2[1/2] \rightarrow 4s^2[3/2]^0$	
	705.9,	738.0,	763.48	$4p^2[3/2] \rightarrow 4s^2[3/2]^0$	
Ar	772.5,	827.3		$4p^2[1/2] \rightarrow 4s^2[1/2]^0$	28
	795.2			$4p^2[3/2] \rightarrow 4s^2[1/2]^0$	
	801.7,	811.6,	842.2	$4p^2[5/2] \rightarrow 4s^2[3/2]^0$	

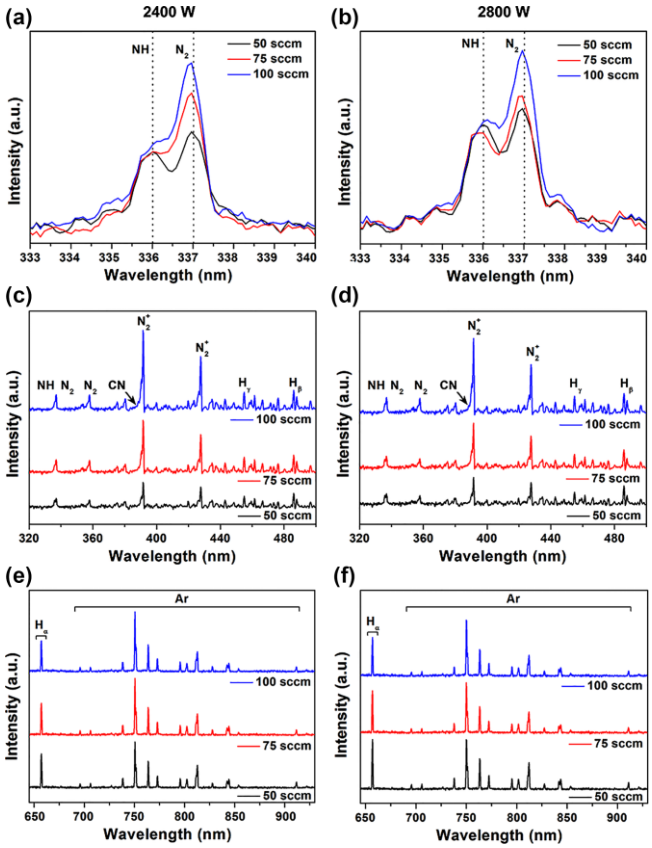

FIG. 11. Optical emission spectra for NH_3 and Ar plasmas at 2400 W, 2800 W and 50 sccm, 75 sccm, and 100 sccm of NH_3 over the wavelength range of (a, b) 333 nm – 340 nm, (c, d) 320 nm – 500 nm, and (e, f) 645 nm – 930 nm.

InN thin film (~39 nm thick) grown at 320ºC and 2800 W was studied by Raman scattering measurements (Fig. 12). Reference spectra from bare Si substrate are also displayed for comparison (bottom curves in each panel). Expanded views of the spectral regions 150–490 cm^{-1}, and 530–650 cm^{-1} are shown in Figure 12 (a–d). According to the factor group analysis six optical modes can be observed for crystalline InN in the first-order Raman spectrum: A_1(TO), A_1(LO), E_1(TO), E_1(LO), E_2(high), and E_2(low).[31] In our Raman scattering experiments, the A_1(TO) and A_1(LO) modes of hexagonal InN were observed at wave numbers of 447 cm^{-1} and 586 cm^{-1} together with peaks ascribed to yet unidentified defects at 180 cm^{-1} and 375 cm^{-1}.[32,33] The band peaking at 436 cm^{-1} is due to second-order Raman scattering from the Si substrate.[34] The sharp rise in parts (c, d) of the Figure 12 is due to the wings of the strong Raman

peak of the substrate at 520 cm^{-1}. Furthermore, the Si-substrate related mode at 520 cm^{-1} has obviously shoulders on the left- and right-hand side that covers the broad range from ~460 cm^{-1} to ~580 cm^{-1} where other phonon modes such as E_1 (TO), E_2^{high} could exist.[35-37] Thereby, the Raman spectra also support that crystalline InN dominated by hexagonal phase was grown on Si.

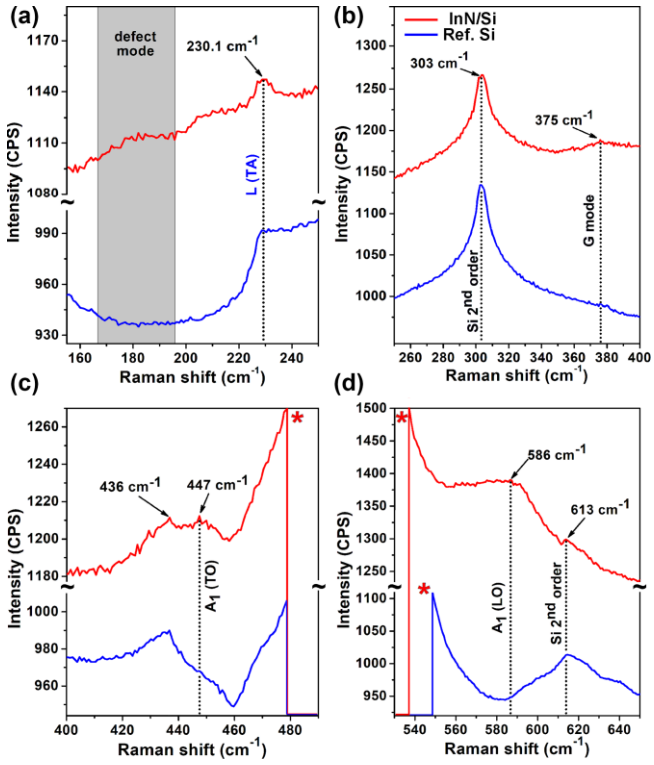

FIG. 12. Raman spectra of InN film grown at 320 ºC and 2800 W of ammonia plasma for 150–250 cm^{-1} (a), 250–400 cm^{-1} (b), 400–490 cm^{-1} (c), and 530–650 cm^{-1} (d). Two prominent modes typical for wurtzite h-InN structure are observed. (* denotes peak from the Si substrate). The bottom curve in each panel displays the spectrum of bare Si substrate in the corresponding region, which serves as a reference.

Using ellipsometric spectroscopy, we obtained refractive index (*n*) and extinction coefficient (*k*) of InN films deposited at 320 ºC and 360 ºC (Fig. 13a). Refractive index was measured to be 2.6 and 2.7 at 650 nm, while it was measured to be 1.95 and 2.03 at 1400 nm, respectively. These values are in good agreement with the reported values for polycrystalline h-InN thin films.[9,38] An increase in thickness of InN from 39 nm to 48 nm leads to an increase in refractive index by 0.1 and 0.08 at 650 nm

and 1400 nm, respectively. This improvement might be attributed to film densification with the increase in thickness of the film. Extinction coefficient (*k*) of InN films, measured to be 0.36 and 0.41 at 600 nm, these values decrease drastically within the wavelength range of 600–900 nm, and reaches rather insignificant level at longer wavelengths.

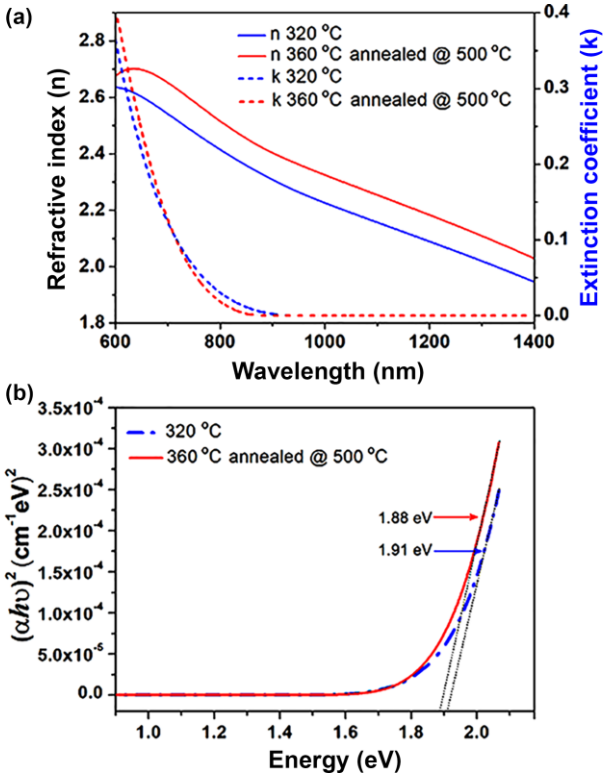

FIG. 13. (a) Optical constants n and k of InN thin film deposited on Si(100) at 320 ºC and 360 ºC. (b) Absorption spectra of the same InN samples.

Figure 13(b) shows $(\alpha h\nu)^2$ vs. hν plot, which is obtained from spectroscopic ellipsometry measurement and related data analysis as explained in the experimental section. Straight line segment of the plot was extrapolated to the abscissa (black arrows shown in the inset of Fig. 13b) which reveals the band edge of InN thin films as 1.91 eV and 1.88 eV at 320 ºC and 360 ºC. These results are in a good agreement to the results (1.9 eV) obtained for InN thin films grown via ALD using TMI and N_2 plasma.[9]

IV. SUMMARY AND CONCLUSIONS

We show the development of a self-limiting InN growth process utilizing trimethylindium and ammonia plasma in a remote plasma ALD system at 240–360ºC and 2400–2800 W plasma power. We find a narrow thermal ALD window between 240 ºC and 260 ºC with a growth rate of 0.36 Å/cycle. The crystalline quality of the InN was found to improve significantly with temperature and self-limiting deposition chemistry was demonstrated also at 320 ºC. The deposited InN films at 320 ºC, 2800 W and 100 sccm of NH_3 flow are polycrystalline by GIXRD with carbon content below 1 at. % and oxygen level below 5 at. % in the film bulk, indicative of a well-functioning ALD surface chemistry. The InN films were found to be nearly stoichiometric by XPS with In/N ratio of 1.1. We ascribe the film bulk oxygen content to film oxidation caused by grain boundary diffusion of oxygen upon exposure to air and possibly also by oxygen containing species possibly formed in the plasma discharge done in a quartz tube. The ammonia plasma was found to contain NH, CN, N_2, N_2^+ and hydrogen radicals by OES. We find that the NH_3 flow through the plasma discharge is an important parameter for depositing films with high crystalline quality and low impurity levels. The refractive index of the InN films was measured to be 2.7 at 650 nm, and 2 at 1400 nm, respectively. The optical band gap of the InN films was measured to about 1.9 eV.

ACKNOWLEDGMENTS

This project was founded by the Swedish foundation for Strategic Research through the project “Time-resolved low temperature CVD for III-nitrides” (SSF-RMA 15-0018) and by the Knut and Alice Wallenberg foundation through the project “Bridging the THz gap” (KAW 2013.0049). IGI acknowledges support from the VR (project VR 2016-05362). PD acknowledges the Carl Trygger Foundation for a post-doctoral scholarship at Linköping University and Laurent Souqui for his kind suggestions during OES measurements.

[1]A. G. Bhuiyan, A. Hashimoto, and A. Yamamoto, J. Appl. Phys. **94**, 2779 (2003).

[2]B. A. Andreev, K. E. Kudryavtsev, A. N. Yablonskiy, D. N. Lobanov, P. A. Bushuykin, L. V. Krasilnikova, E. V. Skorokhodov, P. A. Yunin, A. V. Novikov, V. Yu Davydov & Z. F. Krasilnik, Scientific Reports **8**, 9454 (2018).

[3]S. V. Ivanov, T. V. Shubina, V. N. Jmerik, J. Crystal Growth **403**, 83 (2014).

[4]J. Y. Hwang, C. Park, J. H. Jung, and T. J. Anderson, Journal of The Electrochemical Society **155** (2), H124 (2008).

[5]K. Rönnby, S. C. Buttera, P. Rouf, S. Barry, L. Ojamäe, and H. Pedersen, (2018). Preprint https://doi.org/10.26434/chemrxiv.7067687.v1

[6]S. Ruffenach, M. Moret, O. Briot, and B. Gil, Phys. Status Solidi A **207**, 9 (2010).

[7]H. Peng, X. Feng, J. Gong, W. Wang, H. Liu, Z. Quan, S. Pan, L. Wang, Applied Surface Science **459**, 830 (2018).

[8]A. Haider, P. Deminskyi, M. Yilmaz, K. Elmabruk, I. Yilmazd, and N. Biyikli, J. Mater. Chem. C **6**, 6471 (2018).

[9]A. Haider, S. Kizir, N. Biyikli, AIP Adv. **6**, 045203 (2016).

[10]D. Boris, V. Anderson, N. Nepal, S. Johnson, Z. Robinson, A. Kozen, C. Eddy Jr., and S. Walton, J. Vac. Sci. Technol. A **36**, 5 (2018).

[11]N. Nepal, N. Mahadik, L. Nyakiti, S. B. Qadri, M. J. Meh, J. Hite, and C. Eddy, Jr., Crystal Growth & Design **13**, 1485 (2013).

[12]C. Ozgit-Akgun, E. Goldenberg, S. Bolat, B. Tekcan, F. Kayaci, T. Uyar, A. K. Okyay, N. Biyikli, Phys. Status Solidi C 12, 394**2123** (2015).

[13]M. F. J. Vos, G. Straaten, W. M. M. Kessels, and A. J. M. Mackus, J. Phys. Chem. C **122** (39), 22519 (2018).

[14]D. Shenai-Khatkhate, R. L. DiCarlo, R. A. Ware, J. Cryst. Growth **310**, 2395 (2008).

[15]A. Koukitu, T. Taki, N. Takahashi, and H. Seki, J. Cryst. Growth **197**, 99 (1999).

[16]A. Haider, S. Kizir, C. Ozgit-Akgun, A. K. Okyay, N. Biyikli, J. Vac. Sci. Technol. A, **34**, 1 (2016).

[17]W. Paszkowicz, R. Černý, and S. Krukowski, Powder Diffr. **18**, 2 (2003).

[18]I. Yonenaga, M. Deura, X. Q. Wang et al., AIP Advances **5**, 077131 (2015).

[19]A. Zubrilov, In Properties of Advanced Semiconductor Materials GaN, AlN, InN, BN, SiC, SiGe, (John Wiley & Sons Inc., New York, 2001) p. 49.

[20]G. X. Ju, S. Fuchi, M. Tabuchi, and Y. Takeda: J. Cryst. Growth **370**, 36 (2013).

[21]A. Conde, A.B. Cristóbal, G. Fuentes, T. Tate, J. de Damborenea, Surface & Coatings Technology **201**, 3588 (2006).

[22]C. Cheng, S. Lucas, H. Gutleben, W. Choyke, and J. Yates, Surface Science Letters **273**, L441 (1992).

[23]L. Piper, T. Veal, M. Walker, I. Mahboob, C. McConville, H. Lu, W. Schaff, J. Vac. Sci. Technol. A **23**, 617 (2005).

[24]R. Bazinette, J. Paillol, F. Massines, Plasma Sources Sci. Technol. **24**, 055021 (2015).

[25]L. Yan-qin, B. De-cai, D. Lan-bo, Z. Xiu-ling, L. Zhi-sheng, L. Xue-hui, Spectroscopy and spectral analysis **35**, 765 (2015).

[26]M. Boumerzoug, P. Mascher, P. Mascher, Plasma Chemistry and Plasma Processing **17**, 2 (1997).

[27]C. Vandenabeele, M. Buddhadasa, P. Girard-Lauriault, R. Snyders, Thin Solid Films **630**, 100 (2017).

[28]R. DiMundo, F. Palumbo, F. Fracassi, R. d'Agostino, Plasma Processes and Polym. **4**, S21 (2007).

[29]A. Koukitu, N. Takahashi, and H. Seki, Jpn. J. Appl. Phys. **36**, 136 (1997).

[30]S. Sarapiroma, L. Yua, D. Boonyawana, C. Chaiwonga, Applied Surface Science 310, 42 (2014).

[31]C. A. Arguello, D. L. Rousseau, and S. P. S. Porto, Physical Review **181**, 1351 (1969).

[32]M. Yoshimoto, Y. Yamamoto, and J. Saraie, Phys. Stat. Sol. **7**, 2794 (2003).

[33]J. Wang, Z. Li, P. Chen, W. Lu, T. Yao, Acta Materialia 5**5**, 183 (2007).

[34]A. V. Kolobov J. Applied Physics **87**, 2926 (2000).

[35]M. Liebhaber, B. Halbig, U. Bass, and J. Geurts, Phys. Rev. B **94**, 235304 (2016).

[36]J. Bohn, P. Etchegoin, E. Le Ru, R. Xiang, S. Chiashi, and S. Maruyama, ACS Nano **4**, 3466 (2010).

[37]K. Torii, N. Usukura, A, Nakamura, T. Sota, S. Chichibu, T. Kitamura, and H. Okumura, Appl. Phys. Lett. **82**, 6 (2003).

[38]L. F. Jiang, W. Z. Shen, H. F. Yang, H. Ogawa, Q. X. Guo, Appl. Phys. A **78**, 89 (2004).